Article

Nanosized Tungsten Powder Synthesized Using the Nitridation–Decomposition Method

Qing-Yin He [1], Ben-Li Zhao [1] and Shi-Kuan Sun [2,*]

[1] Foshan Stomatology Hospital & School of Medicine, Foshan University, Foshan 528000, China
[2] School of Materials Science and Hydrogen Energy, Foshan University, Foshan 528000, China
* Correspondence: shikuansun@fosu.edu.cn

Abstract: A facile, one-step nitridation–decomposition method was developed for the synthesis of nanosized tungsten powder with a high surface area. This approach involved the nitridation of WO_3 in NH_3 to form mesoporous tungsten nitride (W_2N), followed by in situ decomposition of W_2N to directly yield single-phase W particles. The phase and morphology evolution during the synthesis were systematically investigated and compared with the carbothermal reduction of WO_3. It was revealed that powdered tungsten product with single-phase particles was obtained after nitridation at 800 °C combined with in situ decomposition at 1000 °C, displaying an average particle size of 15 nm and a large specific surface area of 6.52 m^2/g. Furthermore, the proposed method avoided the limitations associated with intermediate phase formation and coarsening observed in carbothermal reduction, which resulted in the growth of W particles up to ~4.4 μm in size. This work demonstrates the potential of the nitridation–decomposition approach for the scalable and efficient synthesis of high-quality, fine-grained tungsten powder.

Keywords: nanosized tungsten powder; powder processing; morphology evolution; in situ synthesis

1. Introduction

Tungsten (W) is considered to be an important structural material for high-temperature applications. Tungsten possesses a melting point of 3422 °C [1,2], exceeding that of any other pure metal, allowing it to withstand extreme thermal environments. Its high tensile strength of 1725 MPa allows it to resist deformation and breakage under immense loads [3]. Furthermore, tungsten exhibits outstanding corrosion resistance, making it a valuable material for applications involving harsh chemical environments [4]. Coupled with a low thermal expansion coefficient (4.32×10^{-6} K^{-1} at 300 K), it can maintain its dimensions with minimal change under significant temperature changes. This makes it ideal for applications requiring dimensional stability in extreme environments, such as jet engine components and nuclear reactors [5–7]. Moreover, ultrafine tungsten powder is the essential raw material used for the production of ultrafine cemented carbides, widely used in the printed circuit board industry as a component of micro-drilling tools [8,9].

Obtaining high-quality tungsten powder is a critical step in the fabrication of advanced tungsten-based materials [10,11]. The main challenge is focused on densifying the material, often requiring a sintering temperature exceeding 2000 °C. Researchers have explored various methods to synthesize nanoscale tungsten powder, such as high-energy ball milling [12,13], molten salt synthesis [14], and spray conversion processing [15]. Nanocrystalline tungsten powder has been fully densified at temperatures as low as 1400 °C via spark plasma sintering, resulting in an ultrafine-grained microstructure and excellent mechanical performance [16]. However, the most widely-used method is the traditional reduction method [17,18], where tungsten powder is obtained from the reduction of tungsten oxide or ammonium paratungstate (APT) under the flow of hydrogen (H_2). Unfortunately, water vapor produced by the reduction leads to an increase in particle size due to the formation of

volatile $WO_2(OH)_2$, which transports tungsten through the gas phase and promotes particle growth [19]. Therefore, reducing the particle size of the starting powder is a key strategy to lower the densification temperature and achieve a controllable microstructure. This necessitates the development of novel synthesis methods that circumvent the limitations of the traditional hydrogen reduction approach.

As previously reported, a nitridation–carburization method was used to synthesize ultrafine tungsten carbide (WC) powder, in which nitridation of WO_3 using NH_3 and carburization using CH_4-H_2 were conducted sequentially [20]. This two-step process involved the sequential nitridation of WO_3 using NH_3 followed by carburization using CH_4-H_2. Interestingly, the nitridation step resulted in the formation of W_2N, which subsequently transformed into WC powder through carburization at 800 °C. A WC powder was formed with an impressively fine particle size of approximately 20–30 nm. The hypothesis suggested that the initial formation of metallic tungsten occurred via the rapid decomposition of W_2N nanoparticles, a process significantly faster than WO_3 reduction. Rather than the growth and coarsening attributed to the existence of $WO_2(OH)_2$, as mentioned previously, the particle size of WC was be maintained at the nanoscale due to the absence of H_2O in the reaction system. Inspired by this work, an in situ synthesis process was proposed to produce metallic tungsten powder, using a one-step nitridation–decomposition method. This method involved the initial preparation of W_2N intermediate through the nitridation of WO_3 in NH_3, followed by in situ decomposition under an inert atmosphere. The phase and morphological evolution throughout the process were studied. As an alternative method, carbothermal reduction offers the advantages of faster reaction times due to the absence of solid–gas reactions and generally low costs. In the present work, we also attempted to produce tungsten powder via carbothermal reduction of WO_3, and the morphology of the final product and reaction mechanism are compared.

2. Experimental Procedures

A sol–gel route was employed to synthesize WO_3 powder, starting from ammonium metatungstate (Zhuzhou Cemented Carbide Group Corp. Ltd., Zhuzhou, China) and anhydrous citric acid (Sinopharm Chemical Reagent Co., Ltd., Shanghai, China). After gelation, drying, and calcination, nanosized WO_3 precursor with an average particle size of approximately 40 nm was obtained for the following process. More details regarding the procedures can be found in a previous study [20].

The prepared WO_3 powder was placed on a graphite boat and heat-treated in a horizontal tube furnace under a constant flow of NH_3 (600 mL/min) at 800 °C for 3 h to facilitate complete nitridation. Following nitridation, the NH_3 flow was immediately switched to Ar (1000 mL/min) and the temperature was elevated to 900 °C and 1000 °C for in situ decomposition of W_2N to metallic W. The intermediate W_2N after ammonolysis of WO_3 at 800 °C was also collected and characterized.

For carbothermal reduction, the molar ratio of WO_3 to carbon black (purity: 99.9%, Beijing Enoch technology Ltd., Beijing, China) was controlled at 1:2.9. The starting mixtures were mixed for 24 h in a polyethene jar using Si_3N_4 balls and ethyl alcohol as a carrier fluid. The slurry was dried in a rotary evaporator and then moved to a graphite element resistance furnace; the temperature was increased to 1300 °C at 10 °C/min followed by a dwell time of 3 h under vacuum.

The phase assemblage of the as-received powders was investigated using X-ray diffraction with Cu Kα radiation at 40 kV and 40 mA (XRD; Rigaku D/MAX-2 550V, Tokyo, Japan). The mass fraction of W in the mixture of W_2N/W was determined based on the relative intensity of the strongest diffraction peak using the K value method [21]. The reference intensity ratio of W_2N (18.34) and W (18.00) was adopted from JCPDS Card nos. 25-1257 and 89-2767, respectively. Transmission electron microscopy (TEM; JEOL 2100F, JEOL Co. Ltd., Tokyo, Japan) and scanning electron microscopy (SEM; LYRA 3 XMU, Tescan, USA) were used to observe the powder morphology, where the powdered samples from both

3. Results and Discussion

XRD analysis (Figure 1a) confirmed the formation of pure tungsten product through carbothermal reduction of WO_3 at 1300 °C under vacuum, as evidenced by the presence of only tungsten reflections matching JCPDS Card no. 89-2767. This indicated the absence of residual oxides or unreacted starting materials. However, compared to the initial WO_3 powder with an average particle size of ~40 nm [20], TEM images (Figure 1b) revealed the coarsening of W particles after the reaction. The estimated particle size based on TEM analysis was around 0.8 μm, which was further supported by the measured specific surface area of 0.7 m^2/g calculated using the following equation:

$$S = \frac{6}{D \times \rho} \tag{1}$$

where S denotes the surface area, D represents the particle diameter, and ρ is the density. This corresponded to a theoretical particle diameter of 4.4 μm. Notably, the average particle size observed in SEM images (seen in Figure 1c,d) was determined to be within the range of 1–2 μm. Importantly, both XRD and SEM results confirmed the absence of any graphite phase, indicating a complete reaction and no residual carbon black contamination. The TEM observation (Figure 1b) reveals a finer particle structure compared to the SEM images, primarily attributed to the dispersion of the powdered sample onto a Cu grid during TEM sample preparation.
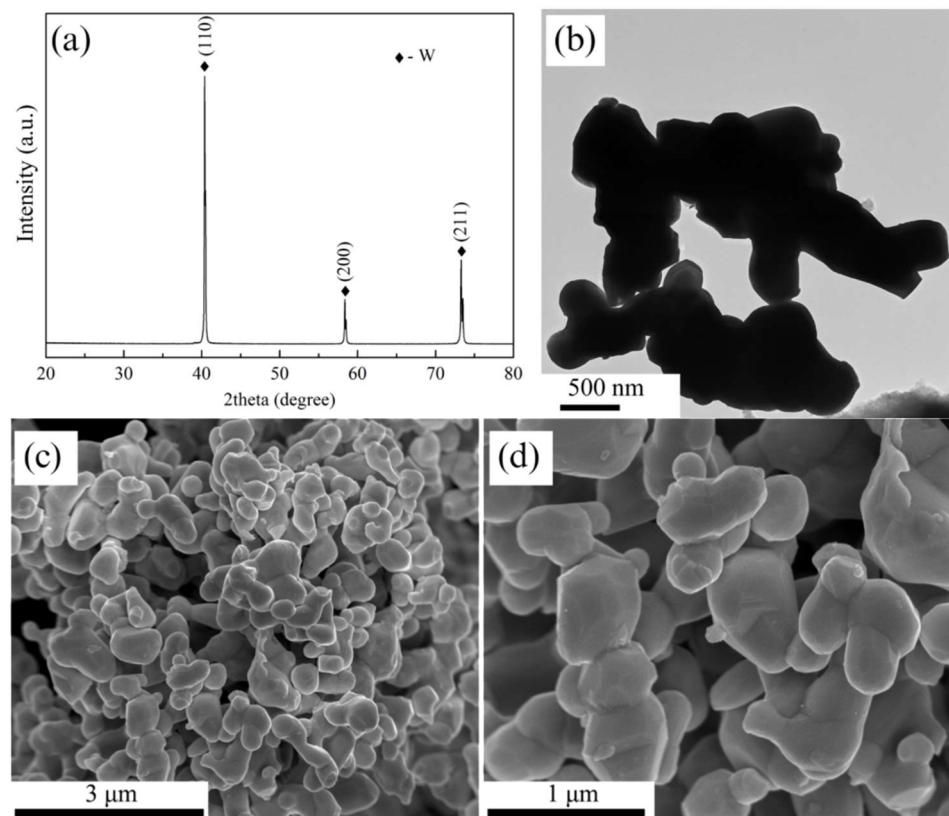

Figure 1. XRD patterns (**a**), TEM (**b**), and SEM observations (**c**,**d**) of the W product after carbothermal reduction of WO_3 at 1300 °C for 3 h under vacuum.

In a previous study, flowing NH_3 was utilized at 600 °C to produce W_2N powder through nitridation of WO_3 [20]. To ensure complete nitridation of WO_3 and prevent

oxygen impurities, the nitridation temperature was increased to 800 °C. Figure 2 presented XRD patterns of the nitrided products, which illustrated phase evolution during nitridation–decomposition of WO_3 at various stages. The dominant phase of the product after ammonolysis of WO_3 at 800 °C was W_2N, as evidenced in Figure 2a by characteristic reflections at (111), (200), and (220). However, the presence of W at $2\theta = 40.0°$ as a minor phase in the product suggests simultaneous decomposition of the nitride intermediate due to the relatively high temperature employed. The W mass fraction was calculated to be 0.9 wt. %. In situ decomposition was subsequently performed by switching the flowing gas from NH_3 to Ar and further increasing the heat-treatment temperature to 900 °C and 1000 °C. As shown in Figure 2b,c, the intensity of W peaks gradually increased with increasing temperature, while those of W_2N decreased. Complete decomposition of W_2N to W was achieved at 1000 °C, as confirmed by the disappearance of W_2N peaks in Figure 2e. Importantly, no intermediate phases were observed during the decomposition process (Figure 2a–e).
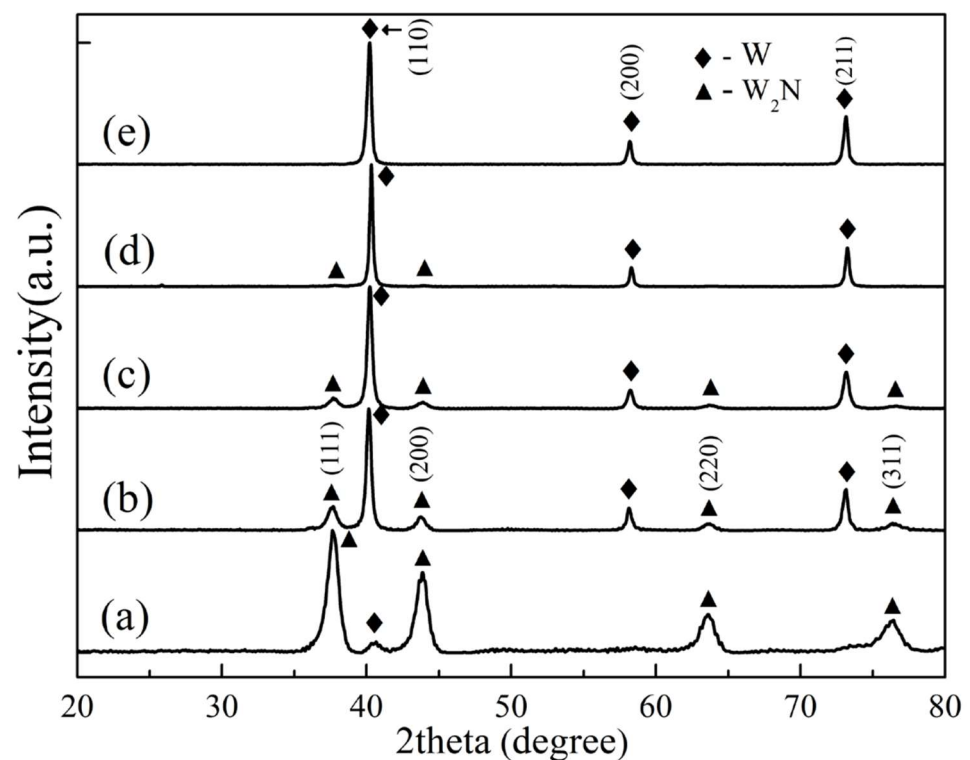

Figure 2. XRD patterns of the intermediate product after nitridation of WO_3 at 800 °C for 3 h (**a**) and in situ nitridation–decomposition at 900 °C for 2 h (**b**) and 6 h (**c**) and at 1000 °C for 2 h (**d**) and 6 h (**e**) in flowing Ar.

The morphology of the W_2N intermediate, obtained from the nitridation of WO_3 at 800 °C for 3 h, is presented in Figure 3a. The particles possessed a near-spherical shape with an average size of approximately 30 nm and exhibited slight agglomeration. Notably, mesopores with a size of approximately 5 nm were observed within the particle structure, as indicated by red arrows in Figure 3b, in contrast to the starting WO_3. The unique formation of mesoporous W_2N was mainly attributed to the nitridation reaction.
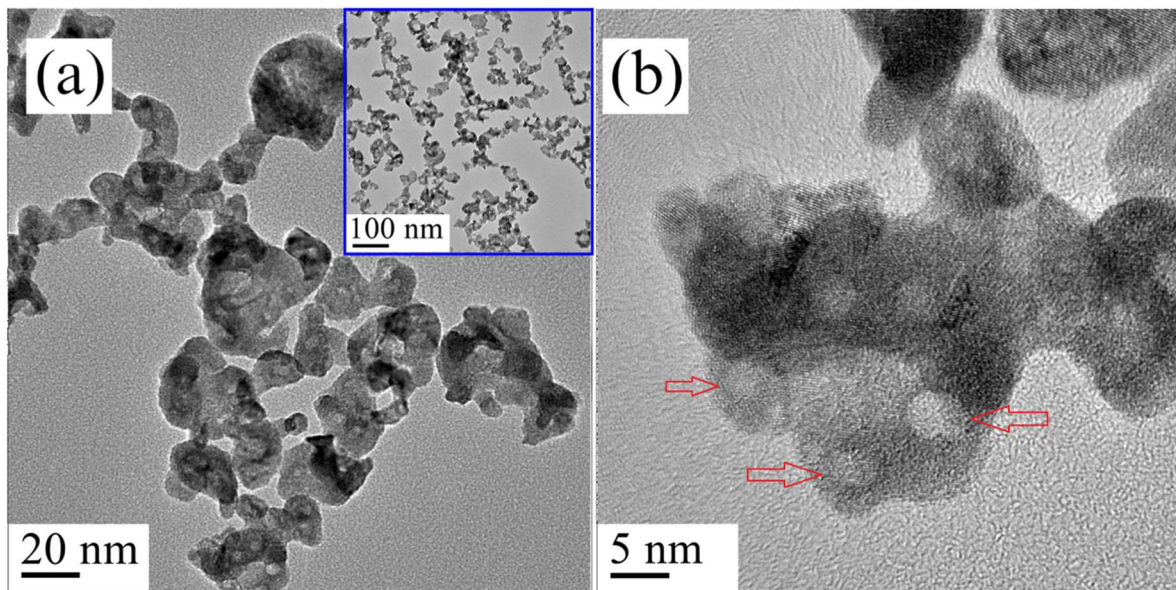
Figure 3. TEM observation of W_2N powders after being heat-treated at 800 °C under low (**a**) and high magnification (**b**).

Tungsten powder derived from the in situ decomposition of W_2N at 1000 °C was analyzed, and the resulting morphology and particle size were investigated. As shown in the TEM observation in Figure 4, the synthesized W powder exhibited a uniform particle size of ~15 nm with narrow distribution. Furthermore, some elongated W particles were observed, possibly originating from the mesoporous W_2N particles. The specific surface area of the W powder synthesized at 1000 °C was measured to be 6.52 m^2/g, indicating a relatively high surface area. In addition, Figure 4b also exhibits that the as-obtained nanosized tungsten powder are bonded together to form some agglomeration. Notably, the particle size of the W product obtained through nitridation–decomposition was smaller than both the raw WO_3 powder and the W product derived from the carbothermal reduction (seen in Figure 1b). This highlighted the potential of this method for synthesizing high-quality, nanosized tungsten powder.
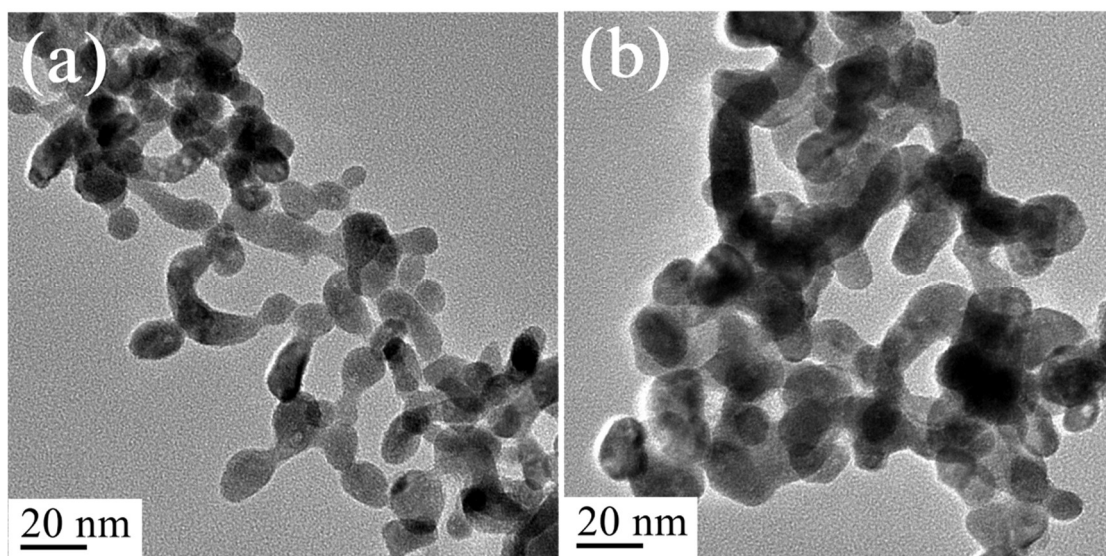

Figure 4. TEM images of W powder after in situ decomposition at 1000 °C in Ar atmosphere showing (**a**) elongated particle, (**b**) agglomeration.

Figure 5 illustrates a proposed mechanism for the morphology changes observed during the nitridation of WO_3. The initial stage involved the formation of a rigid surface layer composed of interconnected W_2N crystallites on the WO_3 particle surface. Due to the great density difference between W_2N (18.1 g/cm^3) and WO_3 (7.28 g/cm^3), a significant volume reduction of up to 67% occurred during the conversion of WO_3 to W_2N. This newly formed nitride layer likely restricted shrinking as the nitridation process continued, consequently, leading to the formation of nanosized pores or cracks within the particles. The W_2N particles formed were comprised of nanocrystalline aggregates, where the mesoporous structure formed within or between these aggregates, which can be observed in Figure 3b. This hypothesis was supported by the variation in the specific surface area. Despite small changes in overall particle size, the W_2N powder exhibits a significantly higher specific surface area (23.63 m^2/g) compared to the starting WO_3 powder (18.10 m^2/g). This increase suggests the development of internal porosity within the W_2N particles, consistent with the proposed mechanism. Due to the crack form within the particle itself, the newly-formed tungsten featured a freshly exposed surface, leading to the formation of soft agglomerates (seen in Figure 4). These agglomerates are expected to be easily broken apart, due to the absence of the water vapor at high temperatures, which would result in the agglomerates of tungsten product derived using the traditional hydrogen reduction method.
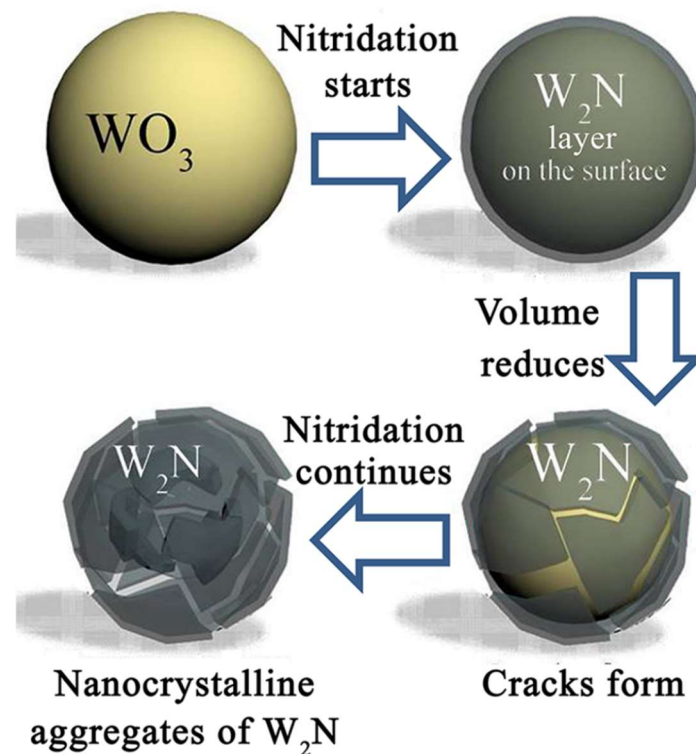

**Figure 5.** Schematic of the mechanism showing morphological changes of WO_3 during the nitridation process.

Although the overall mechanism of the carbothermal reduction reaction of tungsten oxide can be expressed as $WO_3 + 3C = W + 3CO$, the carbothermal reduction of WO_3 to W proceeds through a multi-step reaction mechanism, as previously reported [22,23], namely $WO_3 \rightarrow WO_{2.72} \rightarrow WO_2 \rightarrow W$. In the initial stage, oxygen removal from WO_3 forms intermediate oxides such as $WO_{2.72}$, creating lattice defects that facilitate further reduction. The subsequent reaction between WO_2 and CO produces tungsten and CO_2:

$$WO_2 + 2CO \rightarrow W + 2CO_2.$$
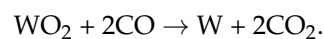
However, it was confirmed that a competing side reaction involving the spontaneous disintegration of WO_2 occurs simultaneously [24]:

$$2WO_2 \rightarrow W + WO_3 + 0.5\ O_2.$$
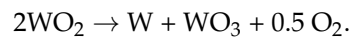
WO_2 was heat-treated under vacuum and WO_3 was identified as the gas phase according to the following reaction [25,26]:

$$3/2WO_2(s) \rightarrow 1/x\ (WO_3)_x\ (g) + 1/2W\ (s).$$
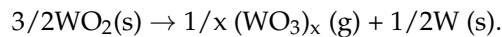
During this process, the highly mobile gaseous WO_3 phase underwent sublimation and was deposited onto the surface of WO_2 or carbon black particles as the carbothermal reduction was occurring. The resulting gaseous $(WO_3)_x$ species contributed to gas-phase diffusion, potentially promoting tungsten particle coarsening via surface energy reduction. Notably, achieving minimal carbon impurities often required non-stoichiometric ratios like $WO_3:C$ = 1:2.9 (used in this study), which presented challenges in precise control due to activity variations in the carbon source.

Unlike carbothermal reduction, the decomposition of W_2N offered a direct route to metallic W with a significantly smaller particle size. This faster process avoided the growth of W particles through chemical vapor transport of tungsten-containing species, as confirmed by the absence of intermediate phases during decomposition. Notably, the direct conversion from nanosized W_2N particles led to inherently smaller W particles compared to the coarsening observed in carbothermal reduction. Table 1 lists the average particle size of W powder obtained through both the nitridation–decomposition approach and carbothermal reduction. The comparison clearly exhibits the particle refinement and advantage for the proposed approach in the present work.

Table 1. Comparison of particle size and surface area of W powder from difference approaches.

Approach	Particle Size (TEM)	BET Surface Area	Feature
Nitridation–decomposition	~15 nm	0.7 m^2/g	Coarsening
Carbothermal reduction	0.8 µm	6.52 m^2/g	Nano-aggregates; mesoporous

Synthesizing high-quality, fine-grained tungsten posed a significant challenge due to the limitations of existing methods. This work directly addressed this need by presenting a novel route for W_2N decomposition, which overcame the drawbacks of particle coarsening originating from intermediate species [26]. Our findings not only offer potential improvements in the densification of tungsten but also open doors for applications demanding a high surface area and precise control over tungsten nanostructures, for instance, in the fields of catalysis [27], nanocomposites [28], and microelectronics [29]. Importantly, further exploration of this method and optimizing reaction parameters and precursor properties hold immense promise for developing an even more efficient and scalable synthesis of fine-grained tungsten. This paves the way for broader adoption of this valuable material in advanced technological applications across various fields.

4. Conclusions

This work successfully demonstrated the potential of an advanced nitridation–carburization method for synthesizing high-quality, fine-grained tungsten powder. Compared to traditional carbothermal reduction, the proposed method yielded W particles with a significantly smaller and more uniform size distribution (~15 nm) and a considerably higher surface area (6.52 m^2/g). This approach offers intriguing possibilities for fabricating advanced tungsten materials, particularly for applications requiring precise control over microstructure and high surface area, such as plasma-facing components in fusion reactors. Furthermore, the presented synthesis method aligns well with the growing demand for

tailored powder materials with specific properties, driven by advancements in fabrication technologies like 3D printing. The rapid processing time and superior product quality suggest the potential for high material throughput upon scaling up the method. Future research should explore the feasibility of integrating this approach with existing production facilities in the cemented carbide industry, aiming to mature and adapt the technology for large-scale production of fine-grained tungsten powder.

Author Contributions: Conceptualization, Q.-Y.H. and S.-K.S.; methodology, B.-L.Z. and S.-K.S.; data curation, Q.-Y.H. and B.-L.Z.; writing—original draft preparation, Q.-Y.H. and S.-K.S.; writing—review and editing, Q.-Y.H., B.-L.Z., and S.-K.S.; project administration, Q.-Y.H. and S.-K.S.; funding acquisition, Q.-Y.H. and S.-K.S. All authors contributed to the article. All authors have read and agreed to the published version of the manuscript.

Data Availability Statement: The original contributions presented in the study are included in the article, further inquiries can be directed to the corresponding author.

Conflicts of Interest: The authors declare that the research was conducted in the absence of any commercial or financial relationships that could be construed as a potential conflicts of interest.

References

1. Klopp, W.D. A review of chromium, molybdenum, and tungsten alloys. *J. Less Common. Met.* **1975**, *42*, 261–278. [CrossRef]
2. Lassner, E.; Schubert, W.-D. (Eds.) The element tungsten. In *Tungsten: Properties, Chemistry, Technology of the Element, Alloys, and Chemical Compounds*; Springer US: Boston, MA, USA, 1999; pp. 1–59.
3. Gumbsch, P.; Riedle, J.; Hartmaier, A.; Fischmeister, H.F. Controlling factors for the brittle-to-ductile transition in tungsten single crystals. *Science* **1998**, *282*, 1293–1295. [CrossRef] [PubMed]
4. Nelson, A.T.; O'Toole, J.A.; Valicenti, R.A.; Maloy, S.A. Fabrication of a tantalum-clad tungsten target for lansce. *J. Nucl. Mater.* **2012**, *431*, 172–184. [CrossRef]
5. Knaster, J.; Moeslang, A.; Muroga, T. Materials research for fusion. *Nat. Phys.* **2016**, *12*, 424–434. [CrossRef]
6. Abernethy, R.G. Predicting the performance of tungsten in a fusion environment: A literature review. *Mater. Sci. Technol.* **2017**, *33*, 388–399. [CrossRef]
7. Omole, S.; Lunt, A.; Kirk, S.; Shokrani, A. Advanced processing and machining of tungsten and its alloys. *J. Manuf. Mater. Process* **2022**, *6*, 15. [CrossRef]
8. Upadhyaya, G.S. *Cemented Tungsten Carbides Production, Properties and Testing*; Noyes Publications: New York, NY, USA; Westwood, NJ, USA, 1998.
9. Sun, J.; Zhao, J.; Huang, Z.; Yan, K.; Shen, X.; Xing, J.; Gao, Y.; Jian, Y.; Yang, H.; Li, B. A review on binderless tungsten carbide: Development and application. *Nanomicro Lett.* **2019**, *12*, 13. [CrossRef] [PubMed]
10. Naito, M.; Abe, H.; Kondo, A.; Yokoyama, T.; Huang, C.C. Smart powder processing for advanced materials. *KONA* **2009**, *27*, 130–143. [CrossRef]
11. Appleyard, D. Powering up on powder technology. *Met. Powder Rep.* **2015**, *70*, 285–289. [CrossRef]
12. Liang, Y.X.; Wu, Z.M.; Fu, E.G.; Du, J.L.; Wang, P.P.; Zhao, Y.B.; Qiu, Y.H.; Hu, Z.Y. Refinement process and mechanisms of tungsten powder by high energy ball milling. *Int. J. Refract. Met. Hard Mater.* **2017**, *67*, 1–8. [CrossRef]
13. Wu, Z.M.; Liang, Y.X.; Fu, E.G.; Du, J.L.; Wang, P.P. The process and mechanisms for the transformation of coarse grain to nanoscale grain in tungsten by ball milling. *Powder Technol.* **2018**, *326*, 222–227. [CrossRef]
14. Zhang, S.; Wen, Y.; Zhang, H. Low temperature preparation of tungsten nanoparticles from molten salt. *Powder Technol.* **2014**, *253*, 464–466. [CrossRef]
15. Kim, B.K.; Lee, G.G.; Ha, G.H.; Lee, D.W. Spray Drying Metal Salts, Desalting, Dehydrating, Milling Metal Oxide Powder, Forming into Green Body, Sintering to Produce Oxide for Use as Alloy Precursor. U.S. Patent No. 5842108A, 14 September 1998.
16. Senthilnathan, N.; Annamalai, A.R.; Venkatachalam, G. Microstructure and mechanical properties of spark plasma sintered tungsten heavy alloys. *Mater. Sci. Eng. A* **2018**, *710*, 66–73. [CrossRef]
17. Luidold, S.; Antrekowitsch, H. Hydrogen as a reducing agent: State-of-the-art science and technology. *JOM* **2007**, *59*, 20–26. [CrossRef]

18. Wu, C. Preparation of ultrafine tungsten powders by in-situ hydrogen reduction of nano-needle violet tungsten oxide. *Int. J. Refract. Met. Hard Mater.* **2011**, *29*, 686–691. [CrossRef]

19. Venables, D.S.; Brown, M.E. Reduction of tungsten oxides with hydrogen and with hydrogen and carbon. *Thermochim. Acta* **1996**, *285*, 361–382. [CrossRef]

20. Sun, S.-K.; Kan, Y.-M.; Zhang, G.-J.; Wang, P.-L. Ultra-fine tungsten carbide powder prepared by a nitridation–carburization method. *J. Am. Ceram. Soc.* **2010**, *93*, 3565–3568. [CrossRef]

21. Madsen, I.C.; Scarlett, N.V.Y.; Kleeberg, R.; Knorr, K. Quantitative phase analysis. In *International Tables for Crystallography*; Gilmore, C.J., Kaduk, J.A., Schenk, H., Eds.; International Union of Crystallography: Chester, UK, 2019; pp. 344–373.

22. Shveikin, G.P.; Kedin, N.A. Products of carbothermal reduction of tungsten oxides in argon flow. *Russ. J. Inorg. Chem.* **2014**, *59*, 153–158. [CrossRef]

23. Gruner, W.; Stolle, S.; Wetzig, K. Formation of CO_x species during the carbothermal reduction of oxides of Zr, Si, Ti, Cr, W, and Mo. *Int. J. Refract. Met. Hard Mater.* **2000**, *18*, 137–145. [CrossRef]

24. Blackburn, P.E.; Hoch, M.; Johnston, H.L. The vaporization of molybdenum and tungsten oxides. *J. Phys. Chem.* **1958**, *62*, 769–773. [CrossRef]

25. Ostermann, M.; Dalbauer, V.; Schubert, W.-D.; Haubner, R. Preparation of nano-crystalline tungsten powders from gaseous $WO_2(OH)_2$. *Tungsten* **2022**, *4*, 60–66. [CrossRef]

26. Schubert, W.D.; Lassner, E. Production and characterization of hydrogen-reduced submicron tungsten powders—Part 1: State of the art in research, production and characterization of raw materials and tungsten powders. *Int. J. Refract. Met. Hard Mater.* **1991**, *10*, 133–141. [CrossRef]

27. Can, F.; Courtois, X.; Duprez, D. Tungsten-Based Catalysts for Environmental Applications. *Catalysts* **2021**, *11*, 703. [CrossRef]

28. Wahlberg, S. Tungsten-Based Nanocomposites by Chemical Methods. Ph.D. Dissertation, KTH Royal Institute of Technology, Stockholm, Sweden, 2014.

29. Inberg, A.; Ginsburg, E.; Shacham-Diamand, Y.; Croitoru, N.; Seidman, A. Electroless and sputtered silver–tungsten thin films for microelectronics applications. *Microelectron. Eng.* **2003**, *65*, 197–207. [CrossRef]